New perspective on the geothermal potential of Wikki Warm Spring, Northeastern Nigeria, from remote sensing and radiometric data

Article *in* Acta Geophysica · April 2023

DOI: 10.1007/s11600-023-01098-1

6 authors, including:

Naheem Banji Salawu
BS Geophysical and Consultancy Ltd.
39 PUBLICATIONS **304** CITATIONS

SEE PROFILE

Akinola Eluwole
Federal University Oye-Ekiti
39 PUBLICATIONS **105** CITATIONS

SEE PROFILE

Fajana Akindeji
Federal University Oye-Ekiti
30 PUBLICATIONS **107** CITATIONS

SEE PROFILE

Muyiwa Michael Orosun
University of Ilorin
87 PUBLICATIONS **958** CITATIONS

SEE PROFILE

Acta Geophysica
https://doi.org/10.1007/s11600-023-01098-1

RESEARCH ARTICLE - HYDROLOGY AND HYDRAULICS

New perspective on the geothermal potential of Wikki Warm Spring, Northeastern Nigeria, from remote sensing and radiometric data

Naheem Banji Salawu[1,2] · Akinola Bolaji Eluwole[2] · Akindeji Opeyemi Fajana[2] · Muyiwa Michael Orosun[3] · Leke Sunday Adebiyi[2,4] · Jibril Olarotimi Salawu[5]

Received: 26 December 2022 / Accepted: 10 April 2023

Abstract

The Wikki Warm Spring is one of the promising locations for the development of geothermal projects in Nigeria. Radiometric and remote sensing data were interpreted to enhance the understanding of the factors controlling the geothermal energy sources in the Wikki Warm Spring. Thus, mapping locations of concealed heat sources offer concentration areas for follow-up geothermal exploration. Landsat-8 imagery was used to produce the land surface temperature (LST) map, which reveals surface temperature variation that ranges from 50 to 95 °C. In comparison, the radiogenic heat map of the region generated from the radiometric data of the study area shows radiogenic heat production rate, which ranged from less than 0.69 to above 3.91 μWm^{-3}. The radiogenic heat and LST maps show similar features, indicating that Basement Complex terrain exhibits high radiogenic and surface temperature than the Benue Trough. Monte Carlo simulation reveals statistical values that suggest that the most likely radiogenic heat value is 1.95 μWm^{-3} around the warm spring, the highest possible (best case scenario) heat value is 2.23 μWm^{-3}, and the least possible value (worst case scenario) is 1.69 μWm^{-3}. The Basement Complex terrain northwest of the warm spring produced high radiogenic heat, generating values above 3.91 μWm^{-3}. The outcome of this investigation is very important for explorationists to institute sustainable geothermal energy mitigation plans and produce a clean and renewable energy in Wikki Warm Spring.

Keywords Remote sensing · Radiometric · Geothermal · Wikki Warm Spring

List of symbols

U	Uranium (ppm)
Th	Thorium (ppm)
K	Potassium (%)
ρ	Density of rock (kg/m^3)
x	Easting (UTM)
y	Northing (UTM)
BT	Brightness temperature for top of atmosphere (Kelvin)
L_λ	Spectral radiance of top of atmospheric (Watts/(m^2 * sr * μm))

Introduction

Interpretation of radiometric and remote sensing data was used to examine the influence of radiogenic heat source on the surface temperature of Wikki Warm Spring and promising locations for geothermal prospecting. Radiometric and remote sensing investigations often render wide-range information on shallow heat source patterns, since the information they provide can cover large areas such as in regional studies presented herein.

Satellite remote sensing technique is highly important in evaluating land surface temperature (LST) variations and monitoring the earth's surface thermal properties (Balew and Korme 2020a). For shallow subsurface investigation, the analysis of aeroradiometric data has been established to be

Edited by Dr. Michael Nones (CO-EDITOR-IN-CHIEF).

✉ Naheem Banji Salawu
salawubanji@yahoo.com

[1] BS Geophysical and Consultancy Ltd, Ilorin, Nigeria

[2] Department of Geophysics, Federal University of Oye-Ekiti, Oye-Ekiti, Nigeria

[3] Department of Physics, University of Ilorin, Ilorin, Nigeria

[4] Department of Physical Sciences, Landmark University, Omu-Aran, Nigeria

[5] Department of Geography, Nigerian Defence Academy, Kaduna, Nigeria

Published online: 26 April 2023

very important in the investigation of subsurface radiogenic heat sources in unexposed regions (Salawu et al. 2021a). The interpretation of radiometric data is very significant in revealing concealed geology of inaccessible regions (Aitken and Betts 2009; Saibi et al. 2016; Salawu et al. 2023). The radiometric method is particularly suitable for revealing the distribution of heat sources since radiometric data are very effective for understanding the heat generation of rock units (Salawu et al. 2021b).

The Wikki Warm Spring comprise of two main elements: heat sources and fluids, which are the carrier of heat-transferring thermal energy. The anomalous heat in the Wikki Warm Spring has its origin from shallow magmatic intrusions (Cratchley et al. 1984; Obande et al. 2014; Abraham et al. 2015). Previous investigations in the Wikki Warm Spring are concentrated on the interpretation of magnetic maps produced from the analysis of aeromagnetic data (Obande et al. 2014; Abraham et al. 2015).

But detailed radiogenic heat source evaluation of Wikki Warm Spring incorporating remote sensing and radiometric data, which would provide more information into the thermal reservoirs of the warm spring are lacking. In addition, the examination of the geological provinces influencing the radiogenic heat sources of the Wikki Warm Spring has not been done, which will enable a proper understanding of radiogenic heat source patterns.

The goal of this present study is to investigate the heat source distributions within Wikki Warm Spring. Mapping both surface and shallow subsurface heat patterns would help localize future geothermal exploration and exploitation projects. Radiometric and remote sensing techniques will be demonstrated by this study to be veritable tools for highlighting such features. Hence, understanding the general geothermal patterns is very vital for the exploitation of hydrothermal fluids within the study area.

Geological setting

The Wikki Warm Spring is located within the Yankari Game Reserve of Bauchi state (Fig. 1). The warm spring attracts international visitors, which makes it a major destination for foreigners and nationals. The spring is among the small number of warm springs within Nigeria, which has a temperature of 31 °C during the day and night, which is higher than the annual average ground surface temperature of 26 °C. The spring lies at 9.75° N and 10.5° E within the study area shown in Fig. 2. The spring is located in the Upper Benue Trough within the Kerri–Kerri Formation (Fig. 2).

The Benue Trough can be sub-divided into three major provinces, which are the Upper, Middle and Lower Benue (Fig. 3); with each province recording separate structural and sedimentary history (Benkhelil 1988; Benkhelil et al. 1998). The initiation and evolution of the Benue Trough can be associated with the opening of the South Atlantic Ocean during the Cretaceous (Mascle 1976; Benkhelil and Robineau 1983; Guiraud and Maurin 1991, 1993). The Benue Trough is an approximately 800 km long NE-trending intracontinental basin, which extends eastward through Bornu Basin to join the African intracontinental rift system. The Benue Trough extends southward to the continental margin, where it is masked by the sediments

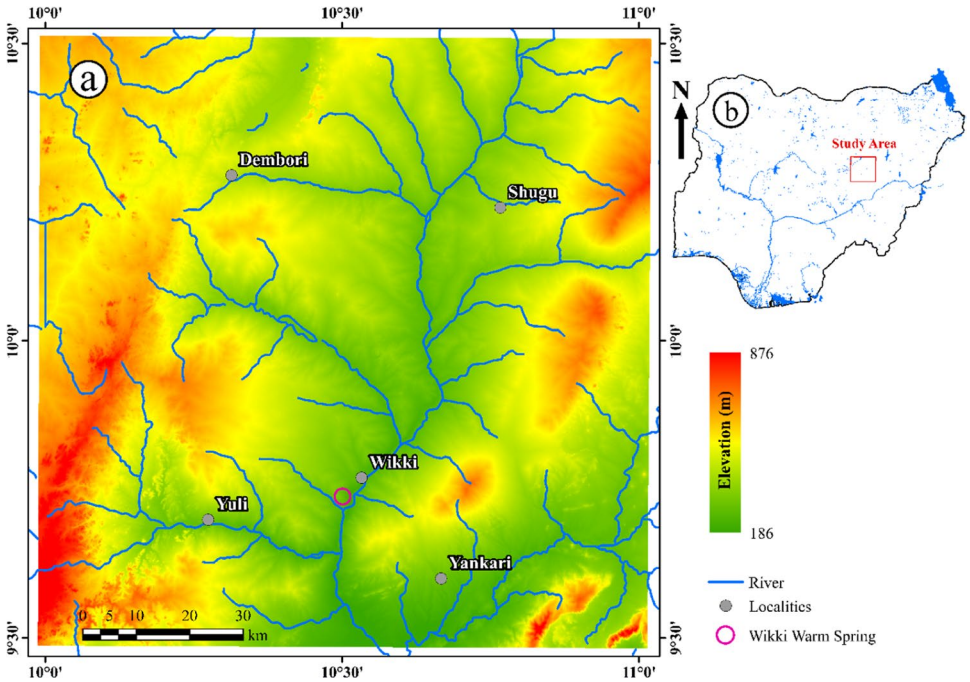

Fig. 1 Location map of the study area: **a** digital elevation model of the study area and **b** insert map showing the location of the study area in Nigeria

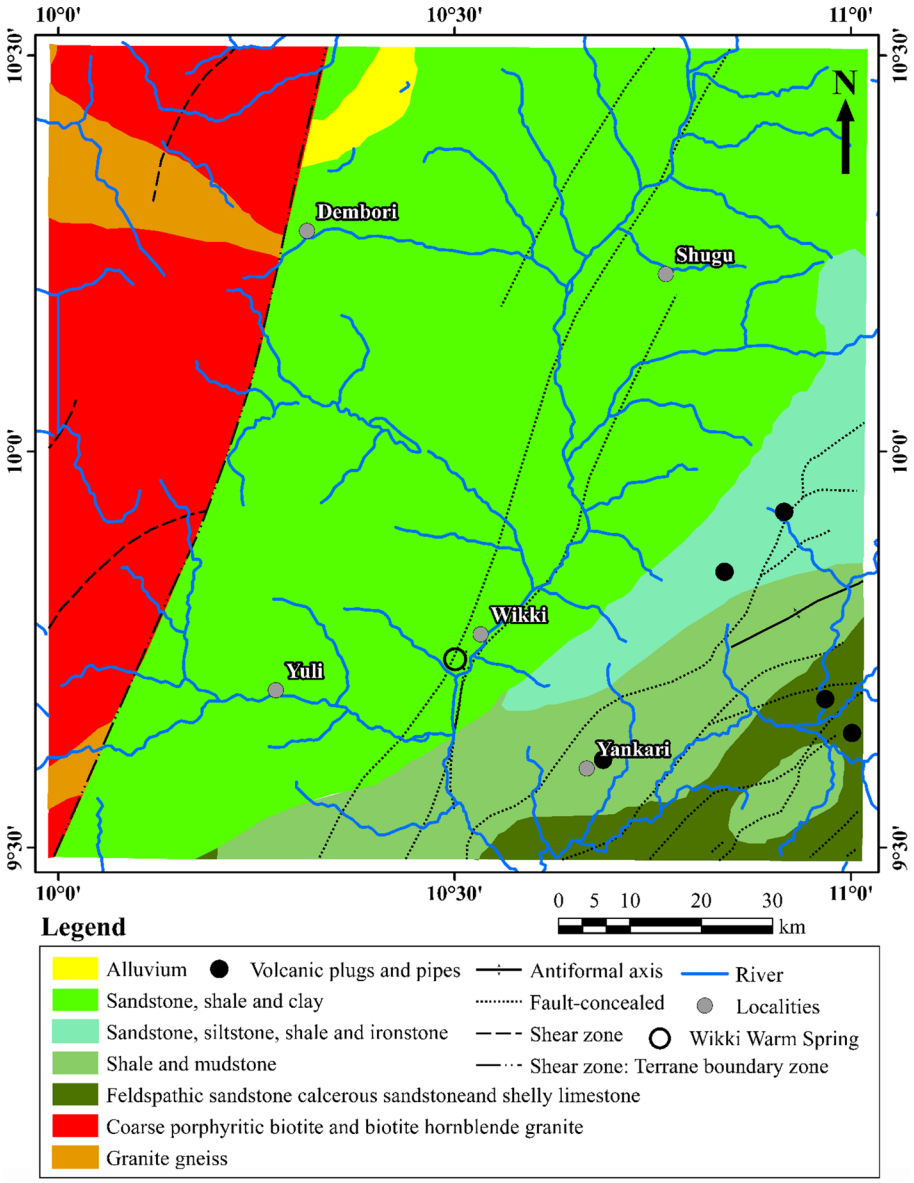

Fig. 2 Geological map of the study area showing location of the Wikki Warm Spring modified from (Geological Map of Nigeria 2020)

of the Niger Delta. It comprises pull-apart sub-basins where rifting and wrenching were active simultaneously (Benkhelil 1988; Guiraud 1993; Benkhelil et al. 1998). All over the world rift zones are well recognized as geothermal active regions and locations where hydrothermal fluids migrate to the surface or near the surface through bounding basin faults (Grauch and Drenth 2009). The sedimentary formations within the Upper Benue Trough form part of the study area (Fig. 3) and unconformably overlies the Archean migmatite-gneiss bedrock. The sedimentary sequence consists of the Bima group, which is covered by the shales of the Pindiga sedimentary formation and Gombe Formation. The Gombe Formation is overlain by the Keri–Keri Formation with both intruded by volcanic rocks.

Data and methods

Data

Two scenes of Landsat-8 operational land imager (OLI) and thermal infrared sensor (TIRS) data covering the study area were used for this investigation. The first scene (LANDSAT_SCENE_ID = "LC81860532021147LG00") was acquired by the Landsat-8 sensors on May 27, 2021 (path/row: 186/53) with a cloud cover of 0.74. The second Landsat-8 scene

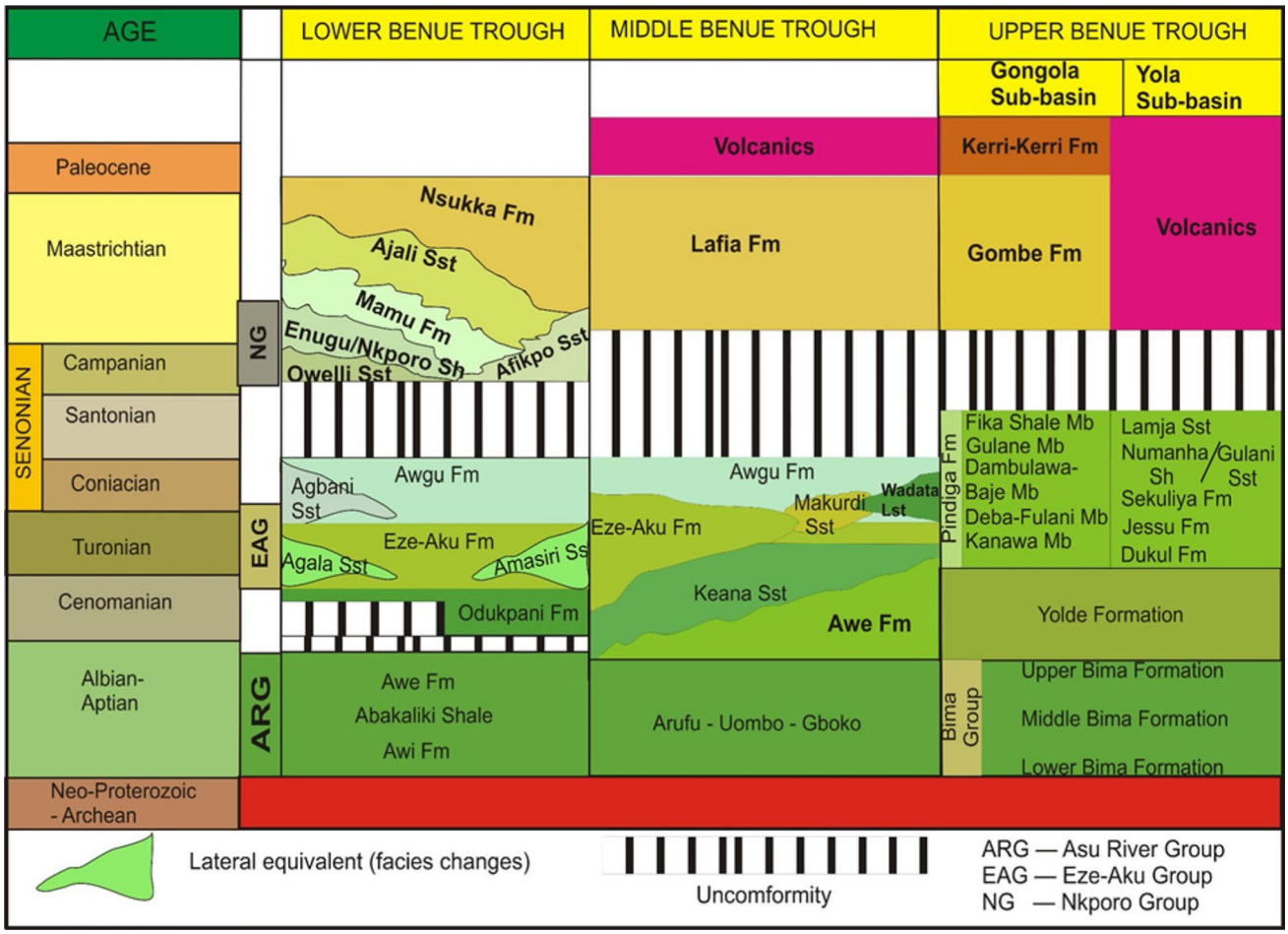

Fig. 3 Stratigraphy sedimentary formations in the Benue Trough of Nigeria (modified after (Carter et al. 1963; Reyment 1965; Offodile 1976; Guiraud 1989; Zaborski 1998; Salawu et al. 2020))

(LANDSAT_SCENE_ID = "LC81870532021154LGN00") was acquired by the sensors on June 3, 2021 (path/row: 187/53) with a cloud cover of 0.03. The two Landsat-8 data were downloaded via the US Geological Survey (USGS) website. The data were acquired in the dry season, which less cloud interference, which certainly improves the visibility of the Landsat-8 sensors, and results in producing images with good geological information. The aeroradiometric data of Wikki Warm Spring were derived from the regional survey carried out by Fugro Airborne Surveys for the Nigerian Geological Survey Agency between 2004 and 2009, which was supported the by World Bank. The gamma-ray spectrometer instrument was utilized for the measurement of the radiometric data (K, Th and U). The airborne radiometric survey was flown along flight lines, which are oriented in the NW–SE directions with line spacing of 500 m, tie line interval of 2 km and sensor mean terrain clearance of 80 m.

Methods

Satellite remote sensing method

The process used to produce the land surface temperature (LST) map of the study area from the Landsat-8 OLI/TIRS bands is given in the steps below using the ArcMap 10.8 software. In addition, a flow chart (Fig. 4) was produced for easy understanding of the steps followed in generating the LST of the studied region.

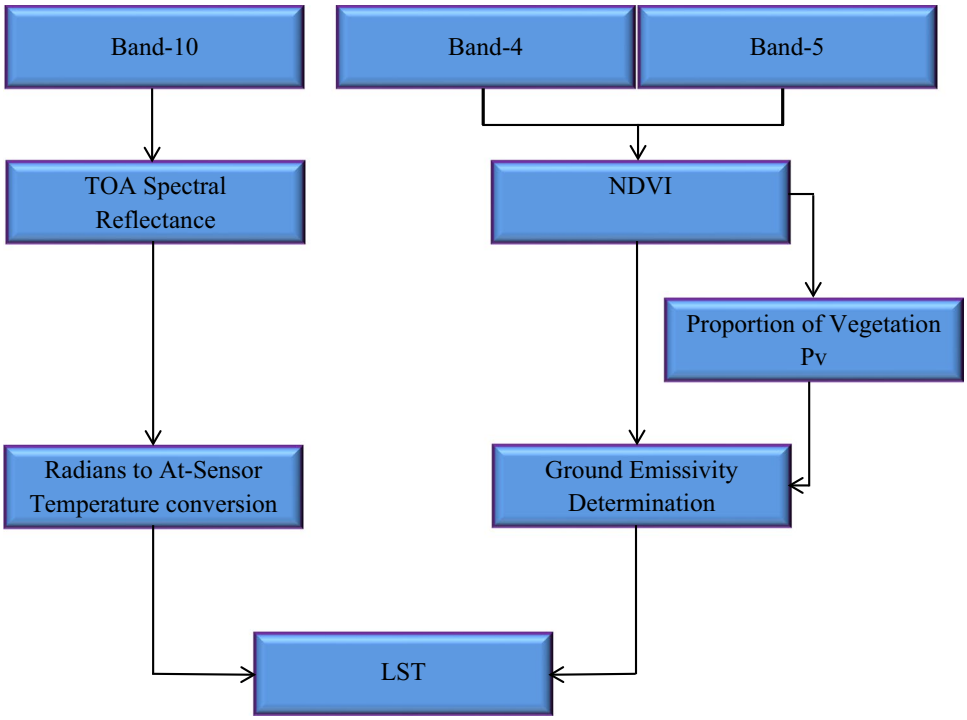

Fig. 4 Flow chart showing how the LST map of the studied region was produced

Conversion to top of atmosphere (TOA) radiance is given in Eq. 1 as (Balew and Korme 2020b):

$$L_\lambda = M_L Q_{\text{cal}} + A_L. \tag{1}$$

Equation 1 is given as:

$$L_\lambda = 0.0003342 * \text{Band } 10 + 0.1, \tag{2}$$

where L_λ = spectral radiance of TOA (Watts/(m^2 * srad * μm)), M_L = multiplicative rescaling band specific factor, A_L = addictive rescaling band specific factor, Q_{cal} = calibrated and quantized standard product pixel values (digital number).

Conversion to brightness temperature (BT) is given in Eq. 3 as (Tan et al. 2010):

$$BT = \frac{K_2}{Ln\left(K_1/L_\lambda + 1\right)}. \tag{3}$$

Conversion of Eq. 3, from Kelvin (K) to degree Celsius (℃), is given as (Avdan and Jovanovska 2016):

$$BT = \frac{K_2}{Ln\left(K_1/L_\lambda + 1\right)} - 273.15, \tag{4}$$

where BT = brightness temperature for top of atmosphere (Kelvin), L_λ = spectral radiance of TOA (Watts/(m2 * sr * μm)), K_1 & K_2 = Constant for band-specific thermal conversion.

Equation 4 is given as:

$$BT = \frac{1321.0789}{Ln\left(774.8853/L_\lambda + 1\right)} - 273.15. \tag{5}$$

The land surface temperature (LST) is given as (Avdan and Jovanovska 2016):

$$LST = \frac{BT}{\left\{1 + \left[(\lambda TB/\rho)\ln \varepsilon_\lambda\right]\right\}}, \tag{6}$$

where LST is given in Fahrenheit, $\lambda = 10.895$, $\varepsilon_\lambda = 0.004 \times \text{Pv} + 0.986$, $\text{Pv} = ((\text{NDVI} + 1)\ /\ (1 + 1))^2$, Pv = proportion of vegetation and $\rho = 1.438 \times 10^{-2}$ mK (Avdan and Jovanovska 2016). The NDVI is defined as Normal Difference Vegetation Index.

Radiometric method

The radiogenic heat of the studied region was calculated from the radiometric data (Fig. 5a, b and c) of the studied region using the Geosoft Oasis Montaj software. The radiogenic heat is given as the total heat per unit volume generated by radioactive isotopes of uranium, thorium and potassium. The heat generated by radioactivity in a unit volume of rock per time is given in μWm^{-3}. The radiogenic heat of the study area was estimated using the (Rybach 1988) equation, given as:

$$A\left(\mu Wm^{-3}\right) = \rho(3.48\ CK + 2.56\ CTh + 9.52\ CU) \times 10^{-5}, \tag{7}$$

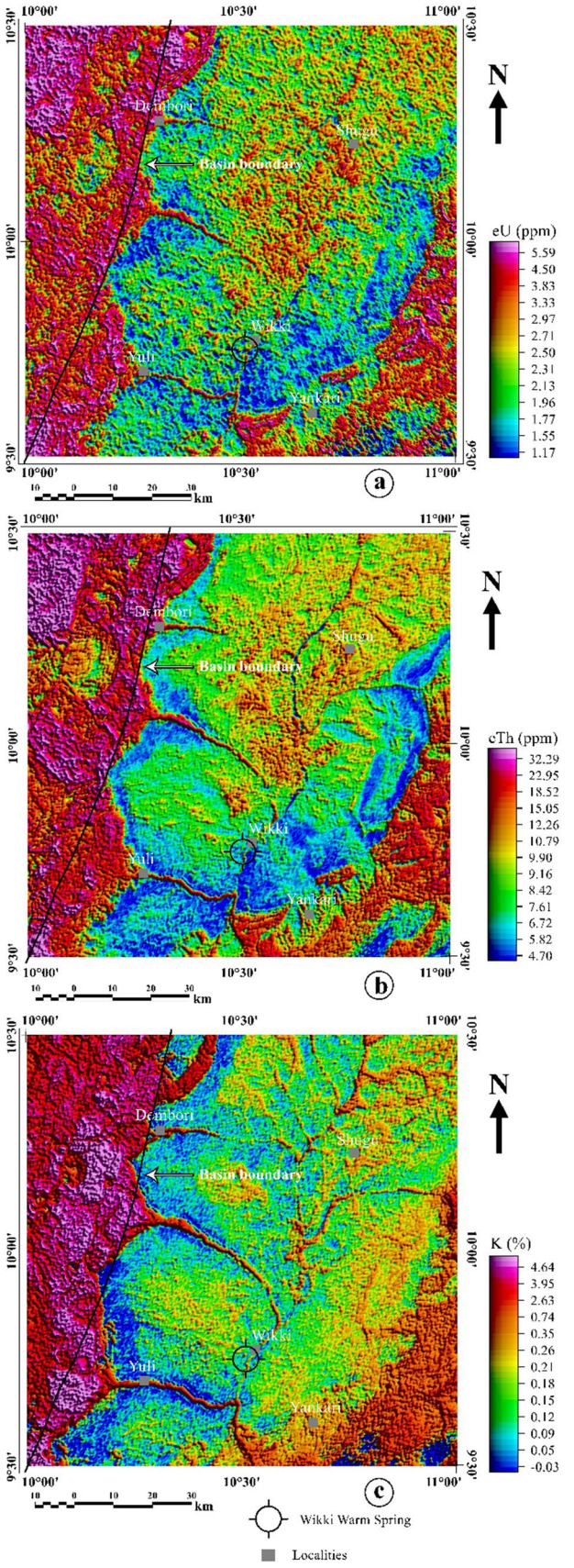

Fig. 5 Radiometric data of the study area used to produce the radiogenic heat map of Wikki Warm Spring and environs. **a** Equivalent uranium map. **b** Equivalent thorium map. **c** Potassium concentration map in percentage

where the density of rock (kg/m^3) is given as ρ and CTh and CU are the concentrations of thorium and uranium in ppm. The concentration of potassium in percentage is given as CK. An average crustal density of 2700 kg/m^3 was used to generate the radiogenic heat map of the study area.

The Monte Carlo simulation approach, which contains a very detailed prediction of the most likely scenario of heat production around the warm spring was successfully employed. This simulation achieves radiogenic heat estimation by producing models, which generate all possible results (probability distribution) through changing arrays of values for factors that contain intrinsic uncertainty (Orosun et al. 2020). The Monte Carlo simulation then calculates the results many times (ten thousand trials for this study), using many random values in the probability function for each event. The Oracle Crystal Ball software version 11.1.2.4.850 was used to perform the Monte Carlo simulations. The estimation of the radiogenic heat values using Eq. 7 is deterministic; thus, it either overestimates or underestimates the actual values of the radiogenic heat. Consequently, a probabilistic approach using Monte Carlo simulation (MCS) that has the advantage of minimizing uncertainty was employed to inspect the probable radiogenic heats associated with primordial radionuclides in the study area. The first step of the MCS is to define hypotheses and give the probability distribution types and parameters of the input variables of the model. The input variables employed in this study are provided in Tables 1 and 2. The uncertain variables in this study include the concentrations of the primordial radionuclides (i.e., uranium (CU), thorium (CTh), and potassium (CK)), the density estimation, the respective weight percentage, etc. The second step was to define the prediction variables according to the equation for the radiogenic heat and then define the number of iterations (10,000) and start the simulation. The final step is to interpret the uncertainty of the predicted variables according to the operation results (Usikalu et al. 2023). In addition, the ternary aeroradiometric map, which is a color combination map was generated by modulating the blue, green and red phosphors in proportion to the uranium, thorium and potassium radiometric data, respectively. The blue color is used for the displaying of the uranium data since the channel has the most noise and the eyes have low sensitivity to the variation in blue color strength (Salawu et al. 2021a).

Table 1 Radiometric data and radiogenic heat values extracted around the Wikki Warm Spring in the black colored circle in Figs. 5 and 7b of the study area

S/N	Easting (x)	Northing (y)	Longitude (DMS)	Latitude (DMS)	Uranium (ppm)	Thorium (ppm)	Potassium (%)	Radioactive heat value (μWm^{-3})
1	665,966.1732	1,075,222.251	10° 30′ 46.5257″	9° 43′ 24.9312″	3.593595667	9.608652768	0.3180496894	1.617529082
2	666,044.6812	1,075,457.776	10° 30′ 49.1360″	9° 43′ 32.5861″	4.233638589	13.03856971	0.4103116544	2.027425984
3	666,123.1893	1,075,827.885	10° 30′ 51.7660″	9° 43′ 44.6216″	4.203189439	13.76300988	0.3974254003	2.068619669
4	666,134.4047	1,076,220.425	10° 30′ 52.1915″	9° 43′ 57.3969″	4.489921739	18.32361634	0.4412721937	2.46145407
5	666,100.7584	1,076,478.38	10° 30′ 51.1254″	9° 44′ 05.7981″	2.948166908	15.68920706	0.4288609068	1.880922369
6	665,977.3886	1,077,117.66	10° 30′ 47.1713″	9° 44′ 26.6243″	2.740558897	11.80973456	0.2741177272	1.545780984
7	666,358.7135	1,077,745.725	10° 30′ 59.7753″	9° 44′ 47.0120″	4.175924793	11.06964585	0.3440933271	1.870094873
8	666,639.0994	1,077,925.172	10° 31′ 09.0015″	9° 44′ 52.8120″	4.309049006	11.02440499	0.3143544811	1.898797404
9	666,863.4082	1,078,093.403	10° 31′ 16.3863″	9° 44′ 58.2550″	3.818223262	9.383395158	0.3033269449	1.657600576
10	668,063.46	1,079,573.841	10° 31′ 55.9819″	9° 45′ 46.2658″	3.906537652	11.2189153	0.4150393921	1.81825226

Table 2 The input parameter for the Monte Carlo simulation. Abbreviation: SD, standard deviation

Parameters	Symbol	Unit	Value Mean ± SD (Min–Max)
Uranium (ppm)	CU	ppm	3.84 ± 0.59 (2.74–4.49)
Thorium (ppm)	CTh	ppm	12.4984 ± 2.80 (9.38–18.32)
Potassium (%)	CK	%	0.3684 ± 0.06 (0.27–0.44)
Density (kg/m3)	ρ	kg/m3	2700 (fixed value)

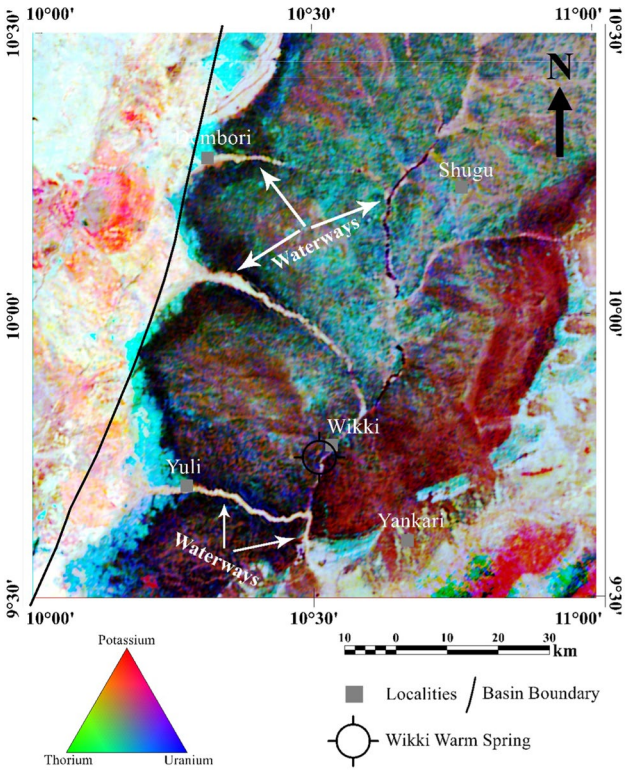

Fig. 6 Radiometric ternary map of the study area generated from the radiometric data of the region

Results

Radiogenic heat

The prepared radiometric maps of uranium (Fig. 5a), thorium (Fig. 5b) and potassium (Fig. 5c) reveal elevated radiometric concentrated zones in the western portion of the studied region that is indicative of high contents of K, Th and U in the basement terrain. This is where the granitic rocks are indicated within the geological map (Fig. 2) of the studied region. The elevated radiometric zone in the western portion of the studied region is more extensive beyond the boundary of the sedimentary basin, which signifies that the granite in the basement terrain extends beneath the sedimentary basin.

The comparison of the ternary map (Fig. 6) with the radiometric maps (Fig. 5a, c) revealed that higher radiometric areas strongly represent granitic rock units in the study area. For instance, the extensive western segment of high radiometric anomalies in Figs. 5 and 6 represents the basement terrain. The white colored areas in the western part of the ternary map showed the extension of the granitic rock units into the sedimentary terrain of the study area. These rock units were covered with the layers of the sedimentary formation as revealed in the ternary map. In spite of the presence of low radiometric anomalies in the sedimentary basin, white elongated color areas are observed in the basin to be closely associated with the river channels in the study area. The observed white areas along river channels may reveal possible exposure of intrusive rocks, which intruded the sedimentary formations in the basin.

Surface and shallow subsurface temperature

The heat pattern within the study area is not consistently very high. Though, the heat pattern is consistent in the

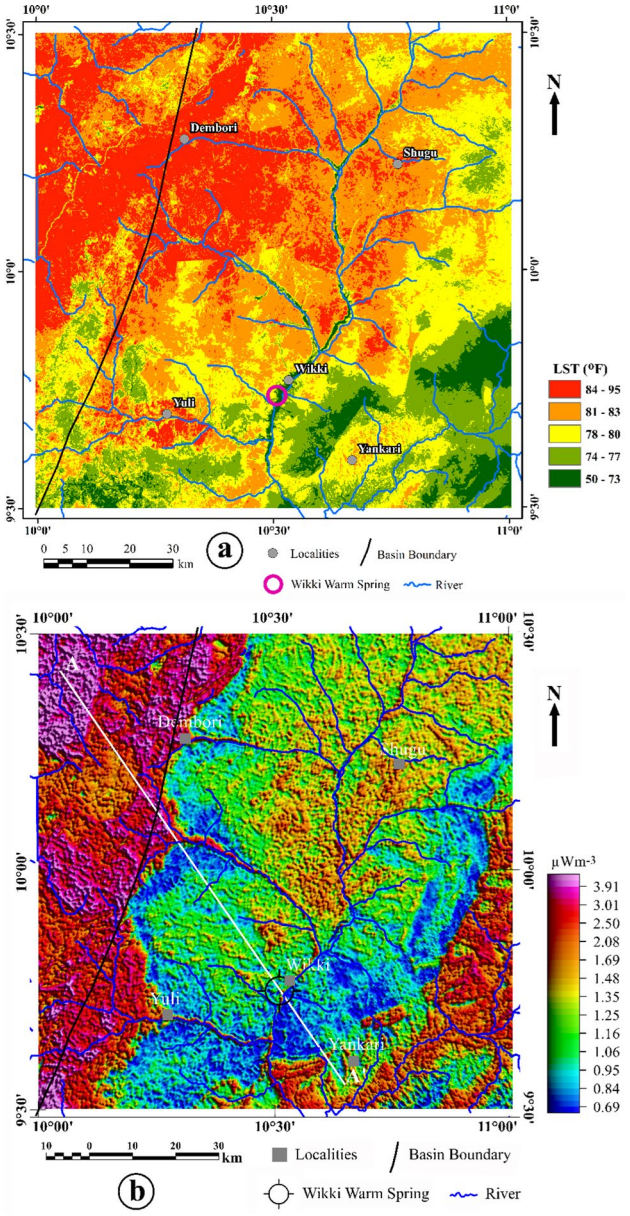

Fig. 7 Comparison between shallow subsurface and surface temperature map. **a** Land surface temperature map of Wikki Warm Spring and environs in degree Celsius. **b** Radioactive heat production rate map in μWm^{-3} with river distribution and profile across Wikki Warm Spring. Profile A-A' is show in Fig. 9a

basement terrain within the western portion of the LST map (Fig. 7a). The LST map reflects the radiogenic heat produced by the granites in the basement terrain. The radiogenic heat map (Fig. 7b) shows that the radioactive elements in the basement terrain exhibit the highest values compared to the eastern portion of the study area that falls within the Benue Trough. The high radiogenic heat within the basement terrain is attributed to higher densities and concentrations of radioactive elements associated with the granites in the basement terrain.

In addition, the radiogenic heat map (Fig. 7b) provides a strong description of near-surface heat based on the temperature variation in the western part of the studied region. It can be detected in the radiogenic heat map that anomalously high temperatures are concentrated in the western portion of the studied region. Furthermore, low to moderate temperature signatures are observed around the Wikki Warm Spring, which signifies that low heat conductivity duvet rocks are around the warm spring. The radiometric data showing the contents of uranium, potassium, thorium and the value of radiometric heat around the Wikki Warm Spring (data extracted within the black circle) are shown in Table 1. Visual investigation of Table 1 reveals that higher radiogenic heat value corresponds with uranium (U = 4.489921739 ppm), thorium (Th = 18.32361634 ppm) and potassium (K = 0.4412721937%), which reveals that the thorium element has the highest influence on the radioactive heat production around the warm spring. The statistical value generated with the Monte Carlo method (Fig. 8) reveals that the most likely radiogenic heat value is 1.95 μWm^{-3} around the warm spring. The Monte Carlo results also indicate that the highest possible (best case scenario) heat value is 2.23 μWm^{-3}, while the least possible value (worst case scenario) is 1.69 μWm^{-3}. The 2-D cross sections (Fig. 9a) show the crossover from the basement terrain to the sedimentary basin where the heat producing granite is buried beneath the high conductive sedimentary formations. However, the duvet sedimentary formations around the warm spring may have low thermal conductivity, which results in low radiogenic heat in Fig. 9a. The low elevation around the warm spring in Fig. 9b is possibly due to fracturing, which creates a pathway for hydrothermal fluids. Following the overall topography of the studied region in Fig. 9c, the hydrothermal fluids are thought to circulate through intrusive rocks, as shown in the conceptual model (Fig. 9d).

Discussion

The distributions of crustal temperature within the crust are dependent on radiogenic and heat sources emanating from the interior of the earth. The location of warm springs such as Wikki Warm Spring within the axis of the BT are indications that unusual hot materials can be found underneath the trough at comparable low depths (Cratchley et al. 1984). In this work, the Wikki Warm Spring geothermal systems are classified utilizing a combination of different criteria, such as the geological setting, the radiogenic heat map and the dominant state of the surface temperature of the region. A conceptual model (Fig. 8d) was developed for the geothermal system in the Wikki Warm Spring to better

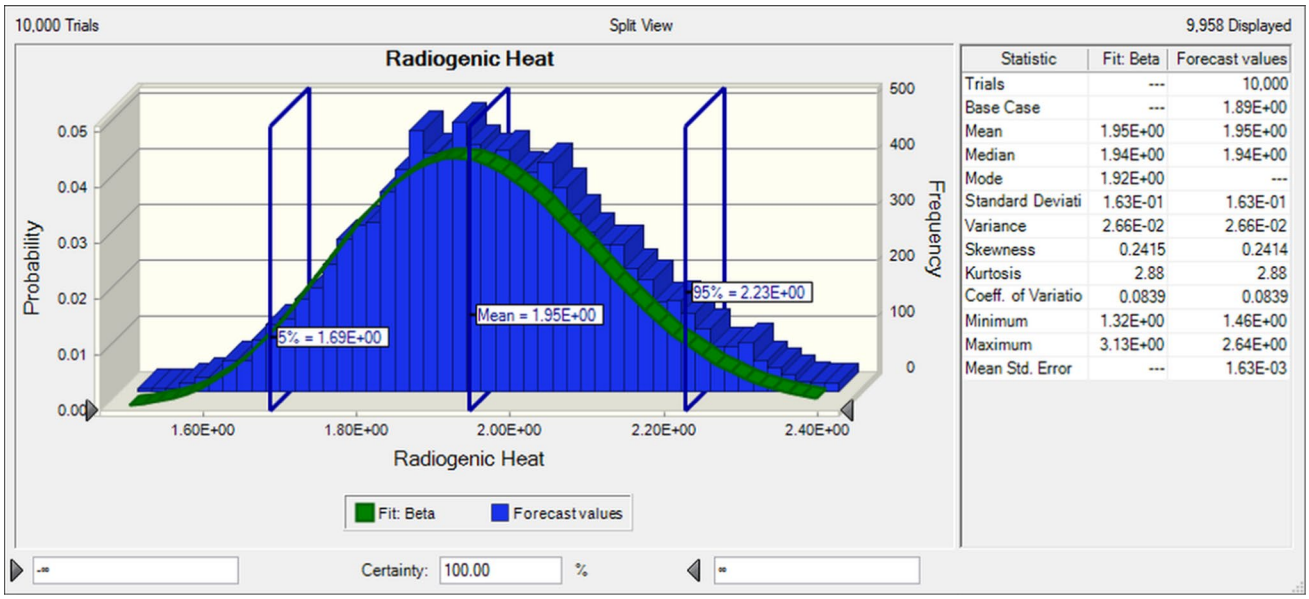

Fig. 8 The Monto Carlo simulation result for the radiogenic heat of Wikki Warm Spring, which was estimated from the radiometric data in Table 1

understand the factors controlling the heat source within the warm spring.

A magnetic analysis study performed by Abraham et al. (2015) attributed the heat sources in the Wikki Warm Spring to magmatic intrusions. Thus, the Wikki Warm Spring heat source is mainly attributed to the intrusions with high content of radioactive elements, which are masked by the less heat conductive sedimentary formations. Our conceptual model proposes that intrusive rock units, within shallow depths, can be a potential source of heat in the Wikki Warm Spring. Based on the results of magnetic analysis, Obande et al. (2014) concluded that the magmatic intrusions in the study area may have caused the heat sources observed in the Wikki Warm Spring.

The result of the aeroradiometric investigation reveals that the basement terrain is enriched with radioactive elements. The radioactive elements contributed to the heat sources within the studied region, which is revealed in the radiogenic heat map. The high radiogenic heat zone corresponds with the high surface temperature areas in the LST map of Wikki Warm Spring and environs. The main volcanic rocks in the western portion of the study area, known as the granites of the Mesozoic Younger Granites series, are in the basement terrain (Fig. 8d).

However, it was shown in the southeastern portion of the studied region that there is an inverse relationship in heat distribution on the LST and radiogenic heat maps compared to the western portion of the studied region as shown in Fig. 7. This inverse relationship where low-moderate LST corresponds to moderate radiogenic heat in Fig. 8 is because the radiogenic heat is duvet by less conductive sedimentary formation, thereby reducing the influence on the land surface temperature.

It was observed in the LST map that the basement complex terrain which falls within the western portion of the studied region has high temperatures, which are attributed to Younger Granites. The lowest temperature zone in the radiogenic heat and LST maps are observed within the Benue Trough southeastern portion of the studied region. This reveals that the sedimentary formations within the Wikki Warm Spring are less conductive to heat. The variation of heat from the western to eastern parts of the study area explains the high relationship between the radiogenic heat map (Fig. 7b) and the geological map of the region (Fig. 2).

The uranium, thorium and potassium elements make various contributions to the radioactive heat generated in rock units within the basement terrain. Examination of the data extracted from the radiometric and radiogenic heat data around the warm spring (data extracted within the white circle in Fig. 5) shown in Table 1, reveals that higher radioactive heat source is mainly correlated with thorium, followed by uranium and potassium. This indicates that the thorium element has a significant influence on the radiogenic heat generation within the warm spring. The utilization of the remote sensing and radiometric techniques defined in this investigation reveals improved knowledge of the study area. The techniques provide an excellent evaluation of radiogenic heat contribution to Wikki Warm Spring. The Monte Carlo approach around the warm spring was utilized to predict the likely radiogenic heat scenario around the

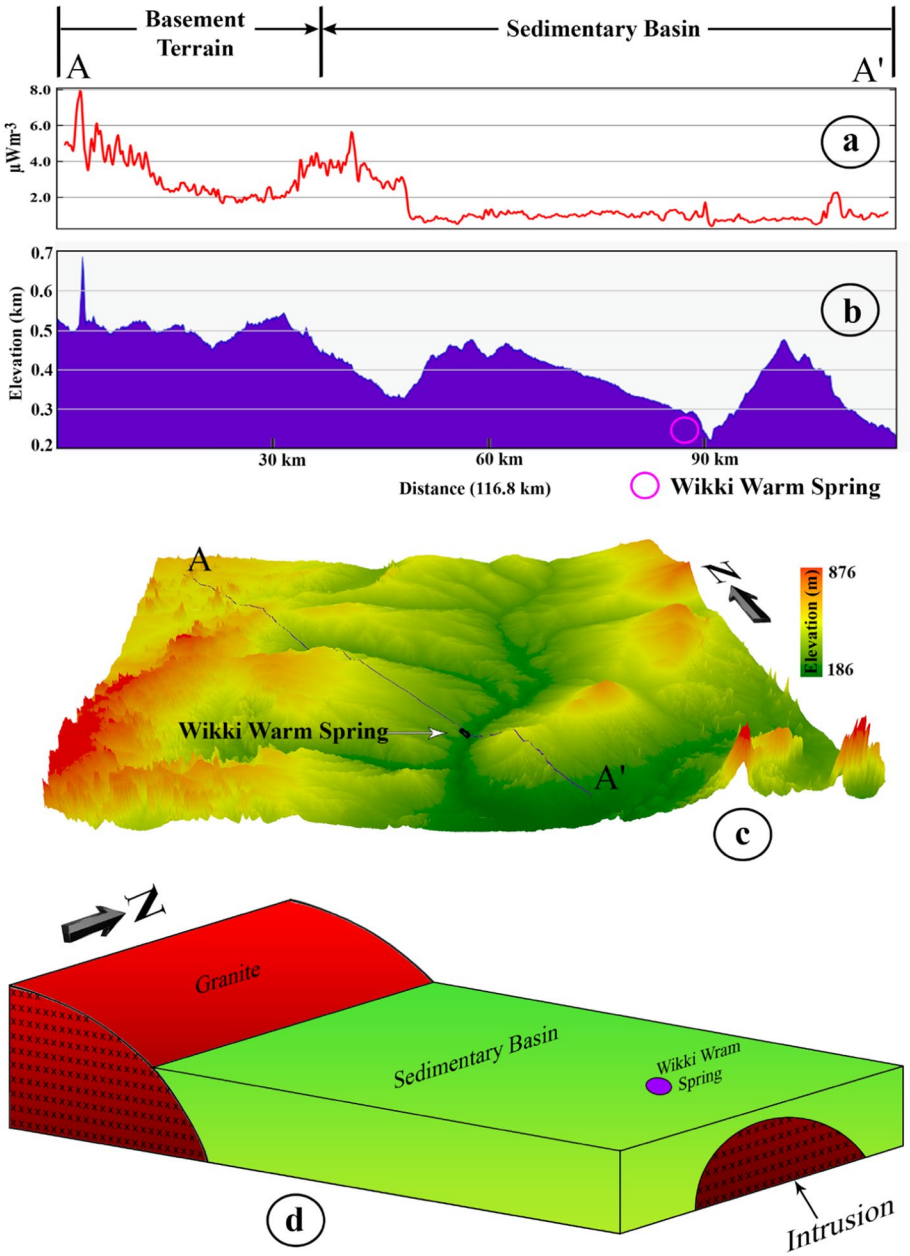

Fig. 9 **a** Radiogenic heat profile across the Wikki Warm Spring, which is indicated in Fig. 7b. **b** Elevation profile across the Wikki Warm Spring. **c** 3-D digital elevation model map of the studied region. **d** Hypothetical model, which shows concealed granite overlain by less conductive sedimentary formation

warm spring (within the white circle in Fig. 5). While the most likely radiogenic heat value is 1.95 μWm^{-3} around the warm spring, the highest possible (best case scenario) heat value is 2.23 μWm^{-3} and the least possible value (worst case scenario) is 1.69 μWm^{-3}. The Basement Complex terrain in the western portion of the studied region in Fig. 7b has the maximum radiogenic heat generating rate, with a high value above 3.91 μWm^{-3}. Accounting for the presence of additional influential features, McCay and Younger (2017) established that any high heat generating (HHG) granitic rock is a granitoid producing heat of more than 5.00 μWm^{-3}; granitic rocks generating heat values ranging from 3.00 to 5.00 μWm^{-3} are categorized as granitic plutons with moderate heat generating rate that will eventually produce direct heat usage instead of very high temperature needed for electrical energy production; and granites with a heat production value low than 3.00 μWm^{-3} are categorized as lower heat generating plutons. This follows that the influence of radiogenic heat source on the surface temperature of the warm spring is significant within the Basement Complex terrain. This shows that the heat source within the warm spring is not only magmatic but also due to radiogenic sources but are duvet by less conductive sedimentary formations. The results from this study show that one of the main factors controlling the heat source in the study area is radioactive elements, which is a new perspective that has not been

explored by previous studies in the region. Hence, this study presents new results on the geothermal potential of Wikki Warm Spring by using a novel approach through the integrated interpretation of remote sensing and radiometric data. Our results will help guide shallow geothermal exploration strategies and have implications for assessing near-surface geothermal potential in Nigeria and other countries. The classification of the geothermal potential of Wikki Warm Spring based on the novel approach proposed in this study should be a starting point for geothermal exploration instead of the last stage of the program. Hence, the results can be further improved for the study area and other regions once more subsurface data such as ground magnetics and gravity, and borehole data are available.

Conclusion

Integrated analysis for the Wikki Warm Spring and environs was carried out utilizing satellite and radiometric data. The statistical value generated with the Monte Carlo method reveals that the most likely radiogenic heat value is 1.95 μWm^{-3} around the warm spring, the highest possible (best case scenario) heat value is 2.23 μWm^{-3} and the least possible value (worst case scenario) is 1.69 μWm^{-3}. This is to characterize the warm spring based on the radiogenic heat source's contribution to the surface temperature of the spring. The interpretation of the Landsat-8 imagery shows the variation of surface temperature that is influenced by radioactive sources. The lowest temperature areas within the study area occurred within the Benue Trough, while the highest surface temperature and radiogenic heat zones occurred within the basement terrain. The high-temperature zones are attributed to granites within the Basement Complex terrain. This indicates that there is radiation of radiogenic heat from buried intrusions in the sedimentary basin to the surface of the study area, especially around the Wikki Warm Spring. The results from this study provided an overall characterization of shallow geothermal prospects around the Wikki Warm Spring. The results also show that one of the main sources of heat in the Wikki Warm Spring is the intrusions, which have high radioactive elements. This study shows that the Wikki Warm Spring is a prospective area for geothermal exploration with shallow heat sources.

Data availability The Landsat-8 OLI/TIRS used for this study is publicly accessible and can be downloaded from the US Geological Survey (USGS) website (https://earthexplorer.usgs.gov/). The coordinates of the study area can be used to download the Landsat-8 data directly from the USGS website. However, the radiometric and aeromagnetic data are not publicly available, but can be acquired from the Nigeria Geological Survey Agency.

Declarations

Conflict of interest The authors have no competing interests to declare that are relevant to the content of this article.

References

Abraham EM, Obande EG, Chukwu M et al (2015) Estimating depth to the bottom of magnetic sources at Wikki Warm Spring region, northeastern Nigeria, using fractal distribution of sources approach. Turk J Earth Sci 24:494–512. https://doi.org/10.3906/yer-1407-12

Aitken ARA, Betts PG (2009) Multi-scale integrated structural and aeromagnetic analysis to guide tectonic models: an example from the eastern Musgrave Province, Central Australia. Tectonophysics 476:418–435. https://doi.org/10.1016/j.tecto.2009.07.007

Avdan U, Jovanovska G (2016) Algorithm for automated mapping of land surface temperature using LANDSAT 8 satellite data. J Sens 2016:1–8. https://doi.org/10.1155/2016/1480307

Balew A, Korme T (2020) Monitoring land surface temperature in Bahir Dar city and its surrounding using Landsat images. Egypt J Remote Sens Space Sci 23:371–386. https://doi.org/10.1016/j.ejrs.2020.02.001

Benkhelil J (1988) Structure et évolution géodynamique du bassin intracontinental de la Bénoué, Nigéria. Bulletin des Centres de Recherches Exploration Production Elf Aquitaine 12:29–128

Benkhelil J, Robineau B (1983) Le fossé de la Bénoué est-il un rift? In: Popoff M, Tiercelin JJ (eds) Rifts et fossés anciens. Bull. Centres Rech. Explor.—Prod. Elf-Aquitaine

Benkhelil J, Mascle J, Guiraud M (1998) Sedimentary and structural characteristics of the Cretaceous along the Côte d'Ivoire-Ghana Transform Margin and in the Benue Trough: a comparison. In: Proceedings of the Ocean Drilling Program, 159 Scientific Results. Ocean Drilling Program

Carter JD, Barber W, Tait EA (1963) Geology of parts of Adamawa, Bauchi and Bornu provinces in Northeastern Nigeria. Geological Survey of Nigeria

Cratchley CR, Louis P, Ajakaiye DE (1984) Geophysical and geological evidence for the Benue-Chad Basin Cretaceous rift valley system and its tectonic implications. J Afr Earth Sci 2:141–150. https://doi.org/10.1016/S0731-7247(84)80008-7

Geological Map of Nigeria (2020) NGSA. Nigerian Geological Survey Agency

Grauch VJS, Drenth JB (2009) High-resolution aeromagnetic survey to image shallow faults. Poncha Springs and Vicinity, Chaffee County, Colorado

Guiraud M (1989) Tectono-sedimentary framework of the early Cretaceous continental Bima formation (upper Benue Trough, NE Nigeria). J African Earth Sci (Middle East) 10:341–353. https://doi.org/10.1016/0899-5362(90)90065-M

Guiraud R, Maurin JC (1991) Le Rifting en Afrique au Cretace inferieur; synthese structurale, mise en evidence de deux etapes dans la genese des bassins, relations avec les ouvertures oceaniques peri-africaines. Bulletin De La Société Géologique De France 162:811–823. https://doi.org/10.2113/gssgfbull.162.5.811

Guiraud R, Maurin JC (1993) Cretaceous rifting and basin inversion in Central Africa. In: Geoscientific Research in Northeast Africa. CRC Press, pp 203–206

Guiraud M (1993) Late Jurassic-Early Cretaceous rifting and Late Cretaceous transpressional inversion in the Upper Benue basin (NE Nigeria). Cent. Rech. Explor.—Prod. Elf-Aquitaine

Mascle J (1976) Le golfe de Guinée: un exemple d'évolution de marge atlantique en cisaillement. In: nouvelle série. Mém. Soc. Géol. France, p 104

McCay AT, Younger PL (2017) Ranking the geothermal potential of radiothermal granites in Scotland: are any others as hot as the Cairngorms? Scott J Geol 53:1–11. https://doi.org/10.1144/sjg2016-008

Obande GE, Lawal KM, Ahmed LA (2014) Spectral analysis of aeromagnetic data for geothermal investigation of Wikki warm spring, north-east Nigeria. Geothermics 50:85–90. https://doi.org/10.1016/j.geothermics.2013.08.002

Offodile ME (1976) A review of the geology of the Cretaceous of the Benue Trough. Geology of Nigeria, Kogbe. C.A. Elizabethan Publishing Co., Lagos, pp 319–330

Orosun MM, Adewuyi AD, Salawu NB et al (2020) Monte Carlo approach to risks assessment of heavy metals at automobile spare part and recycling market in Ilorin Nigeria. Sci Rep. https://doi.org/10.1038/s41598-020-79141-0

Reyment RA (1965) Aspects of the geology of Nigeria. Ibadan University Press, Ibadan

Rybach L (1988) Determination of heat production rate. Handbook of Terrestrial Heat-Flow Density Determination. Springer, Dordrecht, pp 125–142

Saibi H, Azizi M, Mogren S (2016) Structural investigations of Afghanistan deduced from remote sensing and potential field data. Acta Geophys 64:978–1003. https://doi.org/10.1515/acgeo-2016-0046

Salawu NB, Orosun MM, Adebiyi LS et al (2020) Existence of subsurface structures from aeromagnetic data interpretation of the crustal architecture around Ibi Middle Benue Nigeria. SN Appl Sci. https://doi.org/10.1007/s42452-020-2230-5

Salawu NB, Fatoba JO, Adebiyi LS et al (2021) New insights on the Ife-Ilesha schist belt using integrated satellite aeromagnetic and radiometric data. Sci Rep. https://doi.org/10.1038/s41598-021-94813-1

Salawu NB, Fatoba JO, Adebiyi LS et al (2021) Structural geometry of Ikogosi warm spring southwestern Nigeria evidence from aeromagnetic and remote sensing interpretation. Geomech Geophys Geo-Energy Geo-Res. https://doi.org/10.1007/s40948-021-00224-x

Salawu NB, Omosanya KOL, Eluwole AB et al (2023) Structurally-controlled gold mineralization in the southern Zuru Schist Belt NW Nigeria: application of remote sensing and geophysical methods. J Appl Geophy 211:104969. https://doi.org/10.1016/j.jappgeo.2023.104969

Tan KC, Lim HS, MatJafri MZ, Abdullah K (2010) Landsat data to evaluate urban expansion and determine land use/land cover changes in Penang Island, Malaysia. Environ Earth Sci 60:1509–1521. https://doi.org/10.1007/s12665-009-0286-z

Usikalu MR, Morakinyo RO, Orosun MM, Achuka JA (2023) Assessment of background radiation in Ojota chemical market Lagos Nigeria. J Hazard Toxic Radioact Waste. https://doi.org/10.1061/(ASCE)HZ.2153-5515.0000732

Zaborski PM (1998) A review of the cretaceous system in Nigeria. Afr Geosci Rev 5:385–483